EXPERIMENTAL INVESTIGATION OF LASER SURFACE REMELTING FOR THE IMPROVEMENT OF SELECTIVE LASER MELTING PROCESS

Prof. Jean-Pierre Kruth[1], ir. Jan Deckers[2], ir. Evren Yasa[3]
Division PMA, Catholic University of Leuven, Celestijnenlaan 300B, Heverlee, 3001, Belgium
Tel: +32 16 322643 **Fax:** +32 16 322987
[1]Jean-Pierre.Kruth@mech.kuleuven.be, [2]jan.deckers@mech.kuleuven.be,
[3]evren.yasa@mech.kuleuven.be
Reviewed, accepted September 10, 2008

Abstract

Selective laser melting (SLM) is a layer manufacturing process for the direct production of near full density and functional metallic parts with a high geometric freedom. During the process, successive layers of powder are completely molten and consolidated by the energy of a high intensity laser beam. The process is capable of producing almost fully density parts having mechanical properties comparable to those of bulk materials. However, poor surface quality limits the process. This limitation can be overcome by laser surface remelting (LSR) applied on the surfaces having a normal vector parallel to the building axis. Surface modification by LSR does not only improve the surface quality (roughness values more than three times lower), but also has the potential to enhance wear behaviour and microhardness and to change the microstructure. In this study, the parts are first produced by SLM of a Ti-6Al-4V powder. The last twenty layers of the parts are then remolten with different parameter selections using a continuous wave laser source (Yb:YAG). The influence of LSR on surface quality, microhardness, fretting behaviour and microstructure is investigated.

INTRODUCTION

Selective Laser Melting (SLM) is an additive manufacturing technology able to fabricate 3D physical models, parts and tools without almost any geometrical restrictions by stacking and bonding 2D layers in a specified direction (see Figure 1). The process builds up almost 100% dense parts directly from design data using customary metal powder. The parts are built in a layer-by-layer fashion with the metal powder being bonded to the previous layer by locally melting with a high-intensity laser beam that selectively scans the powder bed tracing the layer geometry (see Figure 2a). Compared to other layer manufacturing technologies, SLM has the advantage to produce parts that have mechanical properties comparable to those of bulk materials.

Figure 1. Sample parts produced by SLM: A hollow reinforced part made by Trumpf (a); A heat exchanger as satellite component made by K.U.Leuven (b); An acetabular hip implant cup made by Arcam (c); A dental framework for the support of dental implants made by K.U. Leuven (d).

Although SLM provides many advantages over other manufacturing technologies, it still has some major drawbacks such as insufficient surface quality, stair-case effect, balling, residual stresses and poor dimensional accuracy [1]. Being one of the most important limitations of the process, the insufficient surface quality can be enhanced by employing a variety of surface modification technologies which are available in the market: mechanical processes (machining and abrasive sandblasting), chemical processes (acid etching and oxidation) and thermal processes (plasma spray) [2]. Laser remelting is a valuable alternative to these techniques being a clean and reproducible process with a good controllability of the variables involved in the process. As reported in [3, 4], laser remelting can provide an improvement of 90% in the average and total roughness values of the top surfaces (having a normal vector parallel to building axis) of parts built by SLM. Laser remelting is not only used for surface modifications for lower roughness values [5-8] but also to improve other surface material properties such as microhardness [9-12], friction and wear behavior [12-15], corrosion resistance [16, 17] and wettability [18-20]. Only the studies reported in [3, 4, 8] concentrate on the laser remelting process as a finishing step after an additive process.

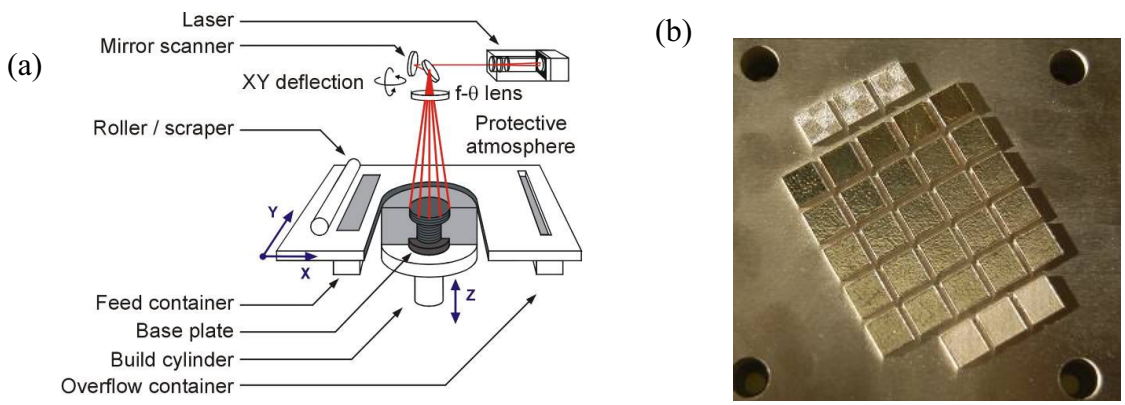

Figure 2.Operating principle of SLM process (a) Test parts built by SLM and exposed to SLR (b)

In this paper, laser surface remelting (LSR) is applied on the last twenty deposited layers of sample parts built by SLM from Ti-6Al-4V powder. This powder is commercially available from Concept Laser. The investigation of the change in the surface roughness is thoroughly reported in [3] and also summarized in this paper since it may be connected to other issues such as microstructure, microhardness and wear behaviour, which are presented in this paper.
The improvement of surface roughness, the change in hardness and the change in wear behaviour by LSR is also studied for SLM parts made from stainless steel powder (ASTM 316L, Concept Laser). Whereas the LSR of Ti-6Al-4V parts is done for the last twenty layers, for stainless steel remelting is only done on the last layer. The investigation of the improvement of surface roughness by remelting stainless steel parts is thoroughly reported in [3, 4]. The study of microstructure, microhardness and wear behaviour of remolten stainless steel parts is reported in another paper.

EXPERIMENTAL PROCEDURE

All sample parts are produced by the LM machine developed at K.U.Leuven. The LM machine employs an Yb:YAG fibre laser with a wavelength of 1085 nm. This laser is only

operated in continuous mode. The maximum laser output power in continuous mode is 300W and the standard beam diameter Φ_{1/e^2} is 50µm.

During the manufacturing of the parts, the last twenty layers were scanned twice. For every one of this twenty layers, the laser beam first melted the powder selectively. Then without laying a new layer of powder, the surface is remolten and this process (layer deposition, SLM, LSR) continued until the part was completed.

The surface roughness of the top surfaces was measured by a roughness tester (Taylor Hobson Form Talysurf 120L). In this paper the roughness of the parts is mostly expressed by the arithmetic mean surface roughness (R_a). The total height of the roughness profile (R_t) and the surface roughness depth (R_z) were also measured and follow the same trend as R_a.

In this study micro hardness measurements are done instead of macro hardness measurements or measurements with a nanoindenter. By not using a macro hardness tester, the measurements could be done relatively close to each other making it possible to investigate the change of hardness of the SLM parts with depth. By not using the nanoindenter, the measurements give a more global overview of the surrounding hardness.
The measurements are done by a Leitz/Durimet vickers microhardness tester. For one hardness measurement, a load of 1.94 N is applied for 30 seconds. The resulting pyramidal indentation, which dimensions are related to the Vicker Pyramid Number [HV], is visualised on a computer screen via a CCD Camera and manually measured by encasing it with a box.
Eight hardness measurements are done to calculate a mean hardness value. Confidence intervals are also calculated, using a confidence limit of 0.95. To investigate the change of hardness of the cross-section of one part as function of depth, eight hardness measurements are done at three different depths (Figure 3-a).

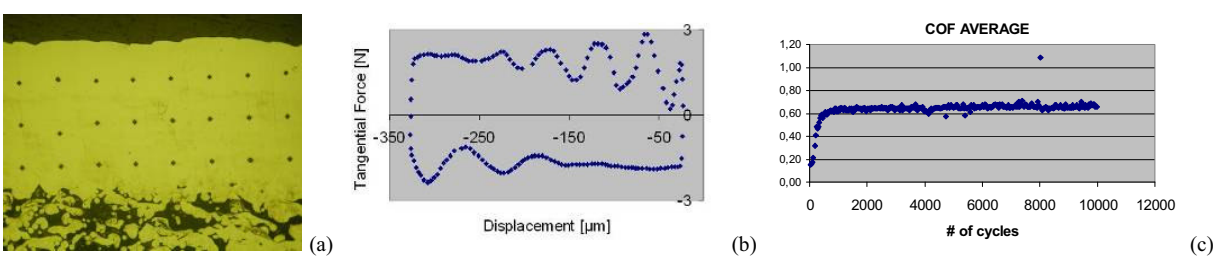

Figure 3: Hardness measurements (a); Fretting test: Tangential force vs. displacement; Coefficient of friction vs. number of cycles (c).

The wear behaviour of the parts is investigated by fretting tests. All tests consisted of 10000 fretting cycles. For the tests a displacement of 350 µm is established between the flat surface of a sample part moving at 6Hz and a fixed corundum ball (diameter 10 mm, surface roughness 0.02). The normal force F_N of 0.2 N was measured and kept constant.
The displacement of the moving table and tangential force F_T is measured every 33th cycle as illustrated in Figure 3-b. From this data the dissipated energy of the cycle E_d is calculated. The coefficient of friction μ_m is calculated from the following formula:

$$\mu_m = \frac{E_d}{2.F_N.d}$$

This formula is only valid when the fretting tests are done in gross slip conditions [21]. To assure this condition the tangential force vs. displacement curve (Figure 3-b) has to be a parallelogram during the entire test. This condition is checked after every fretting test.
After a certain number of cycles, the coefficient of friction always reached a steady state value (Figure 3-c).

The microstructure of the parts made by SLM and subjected to SLE and/or SLR is characterized by an optical microscope and a scanning electron microscope (SEM) using secondary electrons. Before making pictures with the SEM, the parts were polished, etched and covered with a nano-layer of carbon.

EXPERIMENTAL RESULTS AND DISCUSSION

Roughness

P [W] \ V [mm/s]	20	80	320	1280	5120
256	6,9 [2,1]	4,2 [1,2]	4,3 [0,7]	6,4 [1,7]	17,3 [3,6]
128	5,9 [3,8]	5,7 [0,8]	3,6 [1,1]	6,6 [0,6]	14,6 [1,2]
64	17,6 [9,7]	7,6 [2,7]	6,8 [0,8]	12,3 [0,7]	14,0 [0,8]
32	9,7 [1,3]	13,7 [2,2]	14,3 [1,3]	14,5 [1,7]	12,6 [0,9]
16	13,8 [3,1]	16,5 [3,0]	16,9 [1,7]	14,7 [2,0]	12,3 [1,4]

(a)

P [W] \ V [mm/s]	80	160	320	640	1280
256	Ref. 15,7 [3,8]	6,8 [1,1]	7,3 [2,7]	2,9 [0,3]	5,1 [1,1]
181	Ref. 12,7 [1,7]	6,7 [1,4]	5,6 [1,7]	3,7 [0,6]	4,7 [1,0]
128	Ref. 15,4 [0,8]	4,2 [0,4]	4,7 [1,5]	4,8 [1,6]	6,1 [1,6]
91	4,1 [0,5]	5,1 [0,6]	5,8 [0,7]	5,7 [0,3]	7,8 [0,6]
64	4,9 [0,5]	5,1 [0,7]	6,1 [0,4]	7,0 [1,7]	11,5 [2,8]

(b)

Figure 4. Mean roughness [standard deviation] of the Ti-6Al-4V experiments [µm]: First Test (a) Second Test (b)

As a **first test**, 25 parts ($10x10mm^2$) were built to search which set of scan speed and laser power lowers the surface roughness the most. The parts consist of 70 consolidated layers with a thickness of 30 µm. The first 50 layers are scanned using a scan spacing of 74 µm, a laser power of 40 W and a scan speed of 800 mm/s to make a sort of porous, sintered support structure. The last 20 layers are first melted with parameters that are optimised for density: scan spacing 74 µm, laser power 40 W, scan speed 225 mm/s. Each of these layers is then exposed to laser remelting with scan vectors perpendicular to the scan vectors of the melting. Each part is rescanned (remolten) with a different combination of scan speed and laser power. The following scan speeds are used: 20 mm/s, 80 mm/s, 320 mm/s, 1280 mm/s, 5120 mm/s. Each of these scan speeds is used in combination with the following laser powers: 16 W, 32 W, 64 W, 128 W and 256 W. On each part, three 2D roughness measurements were done in the direction of the remelt-vectors. Figure 4-a gives the R_a values (and standard deviations), measured with a gaussian filter and a cut-off of 2.5 mm. The parts that were made with scan speeds between 80 and 1280 mm/s and scan powers between 64 and 256 W have lower roughness values compared to others (see dotted and filled area in Figure 4-a). Notice that settings of 20 mm/s should be avoided, since it retards the built rate of the SLM process.

The window giving low roughness (80 - 1280 mm/s and 64 - 256 W) is further investigated in an analogous **second test**: see settings in Figure 4-b. In this second test, three reference parts were only made with the standard SLM parameters (i.e. 40W and 225 mm/s for the last 20 layers) and not remolten. For an easy overview of the results, the roughnesses obtained for the three reference parts are reported in the three upper-left cells of Figure 4-b. Those cells were empty as no SLR has been applied with 80 mm/s and 128 to 256 W. The cross-section of one of these reference parts is shown in Figure 5-a. For each part three roughness measurements were taken. The results are given in Figure 4-b.

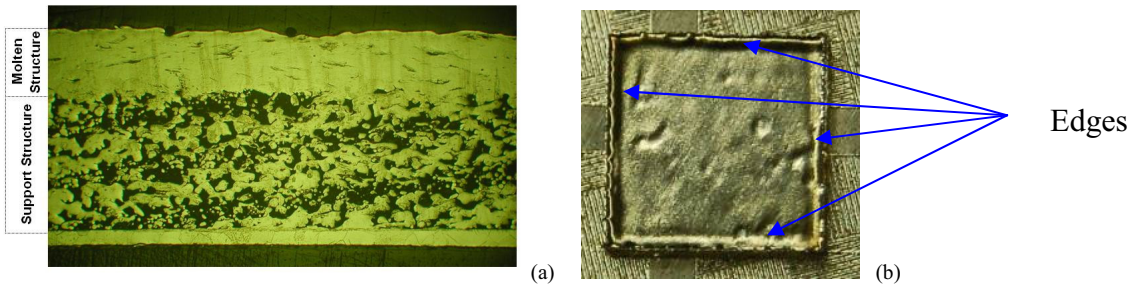

Figure 5. Support structure and molten structure of a reference part (a); Edges (b)

The flatness of the top surface is however affected by the occurrence of edges that arise when the remolten material is partially pushed to the contours of the part by the laser beam (Figure 5-b). These edges that sometimes also occur in pure SLM parts are in general larger if the parts are remolten with a relatively low scan speed and high laser power. To find the power and scan speed that optimizes the given remelting process, an assessment between surface roughness and the size of the edges is necessary. The combinations of scan power and scan speed that give the lowest roughness values with acceptable edges is considered to lie in a diagonal band as marked on Figure 4-b. The most preferable zone of this diagonal band is the one with low roughness values, low edges and high scan speeds (high productivity). The darker the shading in Figure 4-b, the more preferable the remelting parameters.

Microhardness

For 9 parts of test 1 (see dotted cells in Figure 4-a) and two reference parts of test 2 (no SLR, only SLM at 40 W and 225 mm/s), the change in hardness as a function of depth is studied (Figure 6). In particular the change in hardness of the last 20 deposited layers is investigated. These molten and remolten layers have a total thickness of 600 µm.

When using a low remelting power (64 W in Figure 6) in combination with a high remelting scan speed (1280 mm/s in Figure 6), the hardness doesn't change much with depth. In the deeper zones, the hardness seems to be lower than the hardness of the reference parts at the same depth. This assessment suggests a softening of the titanium alloy by rescanning.

When using a higher power or a lower scan speed, the hardness values are always higher compared to the hardness values of the reference parts. By increasing the scan power or decreasing the scan velocity, the hardness values at first increase with depth. A possible explanantion for this phenomenon lies in the fact that a porous support structure has a lower heat conductivity than a fully dense, molten and remolten structure. By rescanning the first layer which is laid on top of the thermal insulating support structure, this surface will achieve a high temperature during remelting (low heat dissipation through porous support structure), yielding

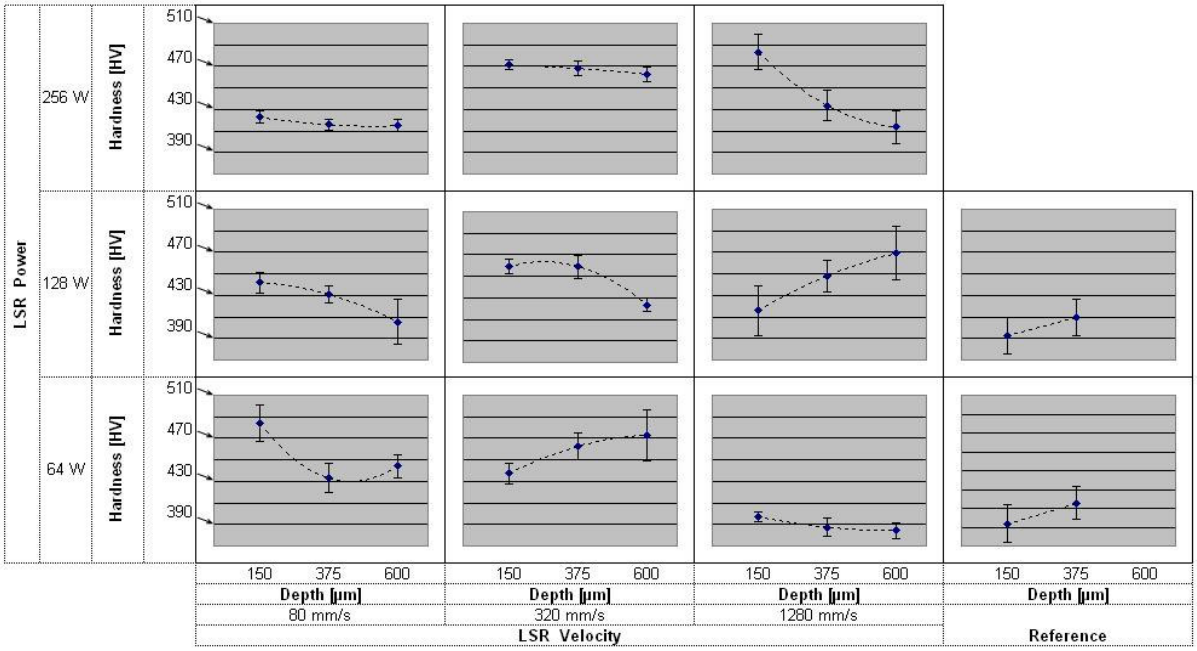

Figure 6. Hardness–depth profiles for 9 parts of test 1 and two reference parts of test 2 [confidence limit: 0.95].

high hardness after quenching. When the twentieth and last layer laid on top of the support structure is rescanned with the same scan parameters, there will be a higher heat conduction of the underlying dense structure. Therefore the surface temperature will be lower and less remelting and hardening will occur. Seemingly, the hardness is more influenced by the higher temperatures reached during remelting than by the lower heat dissipation after remelting (i.e. quenching).

Further increase of the laser power or decrease of the scan speed leads to a more declining trend of the hardness versus depth. Now the scan parameters seem to induce such high amount of energy that not only the top surface is remolten but also softening of the underlying structure occurs.

When a very high scan power is used together with a low scan speed, the hardness again doesn't change much with depth. The heat affected zone seems to be too large to have a change of hardness in the first 600µm under the surface.

Wear behaviour

The parts of test 2, exept two of the three reference parts used for the cross-sectional hardness measurements as mentioned in the previous paragraph, are first polished to eliminate the infuence of the surface roughness in the study of the wear behaviour by fretting tests (Figure 7-a, Figure 7-b). Three fretting tests are carried out on the reference part and the parts remolten with scan velocities 80 mm/s, 320 mm/s and 1280 mm/s and laser powers 64 W, 128 W and 256 W. Only one fretting test is carried out on the other parts.

To determine the volume of the material removed by the fretting tests, all wear-scars of the fretting tests are quantified using a surface profilometer (Wyko NT3300, Figure 7-c). The hardness is measured at eight different places around the wear-scar (Figure 7-d).

A few hardness measurements are done in a scar. This measurements reveal that the dark zones of the scar in Figure 7-d are softer (±381HV) than the bright zones (±541HV).

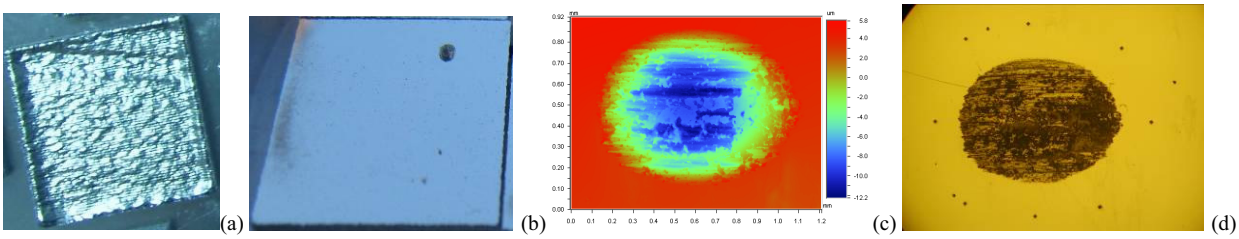

Figure 7. SLM part before polishing (a). Scar of a wear track after polishing (b), quantified by a surface profilometer (c) or seen together with surrounding hardness measurements through an optical microscope (d).

The most fretting tests are done for the parts that are remolten with a scan velocity of 320 mm/s or 1280 mm/s. Figure 8 plots the wear volume vs. the hardness for these velocities. The figure reveals that for a constant remelting scan velocity, the wear volume of a scar might be proportional to the hardness of the surrounding top surface.

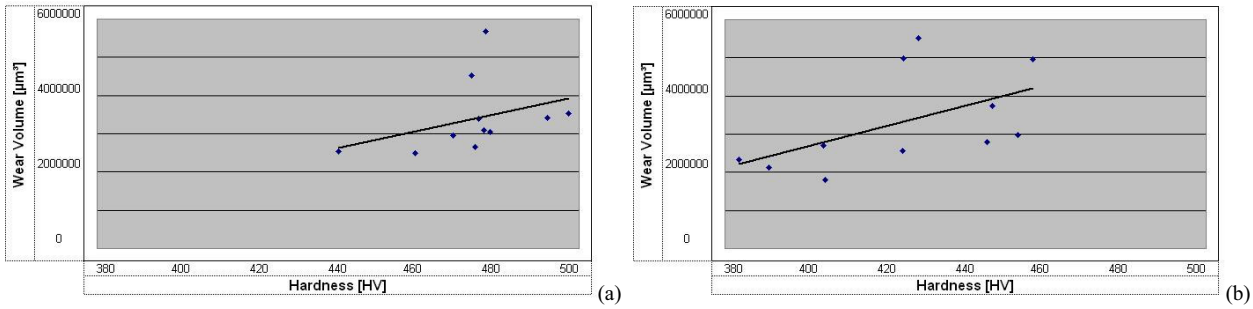

Figure 8. Wear volume vs. hardness for parts remolten with scan velocities 320 mm/s (a) and 1280 mm/s (b).

As already mentioned, on some parts three fretting tests are carried out and the volume of the resulting wear-scars are measured. The variation of wear volume seems to be larger for parts that are not rescanned (reference part) or rescanned with low energy density (e.g. laser parameters: 1280 mm/s and 64 W) than for the parts that are rescanned with high energy density (e.g. laser parameters: 320 mm/s and 256 W). E.g. the wear volumes of the three fretting tests which are carried out on the reference part are 16.4×10^5 µm³, 42.6×10^5 µm³ and 62.7×10^5 µm³. The wear volumes of the three fretting tests wich are carried out on a part which is remolten with a high energy density (laser parameters: 320 mm/s and 256 W) are 26.4×10^5 µm³, 30.8×10^5 µm³ and 33.9×10^5 µm³.

Microstructure

Figure 9a-c gives a cross-sectional view of one of the three reference parts made in test 2. The difference in porosity between the first 50 layers and the last 20 layers is clearly visible through an optical microscope (Figure 9-a). By etching the part ghost-shaped structures become visible by optical microscopy (Figure 9-a) and by scanning electron microscopy (SEM, Figure 9b-c). The same structures appear when remelting with a relatively low power and a high velocity (e.g. laser remelting parameters: 128W and 640mm/s). It is also remarkable that this kind of structures sometimes appear around pores, suggesting that it may be formed by oxides. X-ray diffraction analysis (XRD) are needed for a more detailled investigation of this phenomenon.

Remelting with a higher scan power and/or a lower scan speed leads to the formation of some grain-like patterns or structures and an improvement of the part density. Figure 9d-e illustrates that if an extremely high energy density is used for the remelting (e.g. by choosing a high remelting power of 256W and a low scan speed of 80 mm/s), the porous support structure almost disappears due to an increase of the heat affected zone (HAZ).

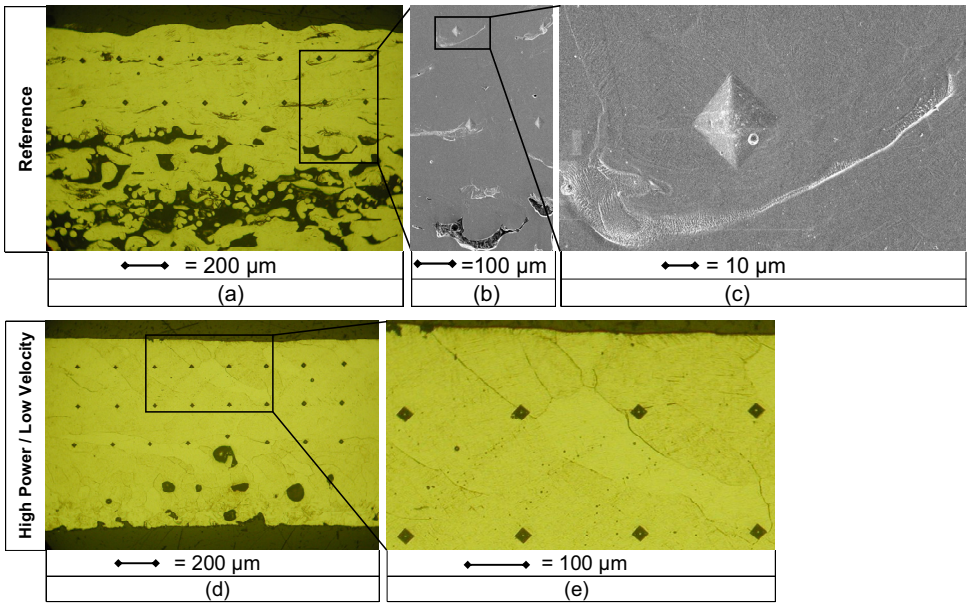

Figure 9. Change of microstructure according to remelting parameters: No remelting [= low scan power and high scan velocity] (a, b, c); High scan power and low scan velocity [256W, 80 mm/s] (d, e);

Similar grain-like structures also appear when surface remelting stainless steel parts produced by SLM. Due to lack of space for a detailed description of the results obtained by SLM and SLR of stainless steel parts, those details are skipped here, but will be published in another paper.

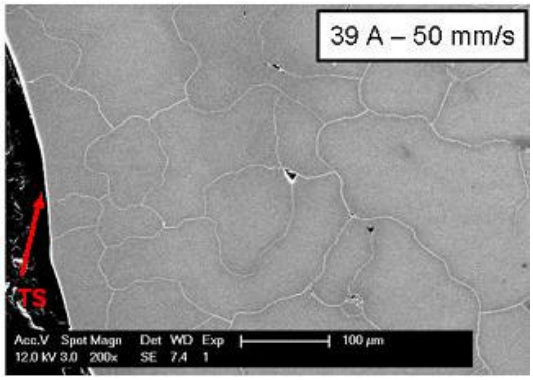

Figure 10. SEM-picture of a cross-section of surface remolten stainless steel part (TS = top surface)

All the parts investigated by the SEM consist of needle shaped structures. The needle shaped structures are also visible in SEM-pictures taken from the pyramidal indentations of the hardness measurements (Figure 11). As this figure illustrates the hardness seems to increase when the texture of the needles becomes finer. The subfigures Figure 11-a, Figure 11-b and Figure 11-c show structures that might be called in literature respectively Widmanstätten, coarse martensitic

and fine martensitic. Widmanstätten, coarse martensitic and fine martensitic structures are formed when respectively higher cooling rates or less softening by reheating is established [25-30]. This indicates a correlation between the thermal history of the material and the measured hardness. XRD analysis need to be done and backscattered SEM images of unetched, polished samples need to be examined to investigate this further.

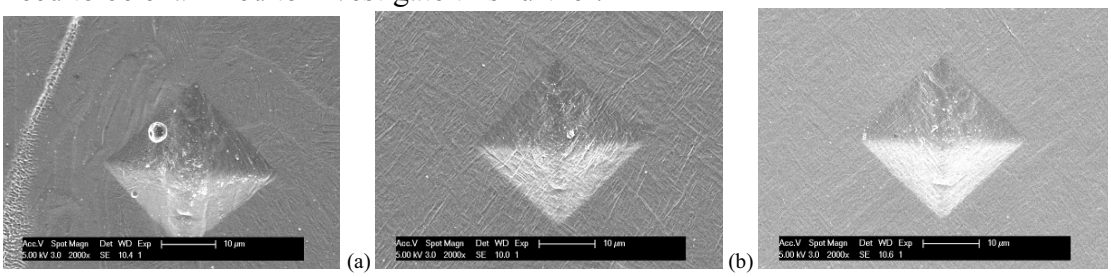

Figure 11. Change of hardness according to change of microstructure: 396HV (a), 434HV (b) and 469HV (c).

Discussion

For a semi-infinite body of isotropic material scanned (rescanned/remelted) with a moving Gaussian laser beam, the following relation describes the evolution of the normalized peak surface temperature T_p^* versus the normalized laser power q^* and normalized scan velocity v^* [28].

$$T_p^* = \left(\frac{1}{\pi}\right)^{\frac{3}{2}} . q^* .\arctan\left(\left[\frac{8}{v^*}\right]^{\frac{1}{2}}\right), \text{ with } T_p^* = \frac{T_p - T_0}{T_m - T_0},\ q^* = \frac{A\ .\ q}{r_B.\lambda.(T_m - T_0)} \text{ and } v^* = \frac{v\ .\ r_B}{a} \qquad (1)$$

where A is the material absorptivity, q is the incident laser power, r_B is the beam radius (= $\Phi_{1/e^2}/2$), λ is the thermal conductivity, T_m is the melting temperature, T_o is the initial temperature, T_p is the peak surface temperature when the laser passes along, v is the scan speed and 'a' is the thermal diffusivity.

As an example, in this paragraph material properties of titanium alloy are used together with scan speeds varying from 80 mm/s to 1280 mm/s. This corresponds to a normalized scan speed v^* varying between 0.73 and 11.8 respectively. For this region formula (1) can be approximated by

$$T_p^* = \left(\frac{1}{\pi}\right)^{\frac{3}{2}} . q^* . \left[\frac{8}{v^*}\right]^{\frac{1}{2}} \qquad (2)$$

This formula suggests that the peak surface temperature is proportional to the laser power and the square root of the inverse of the scan speed.

Every diagonal in Figure 4-b represent parts that are remolten with a constant $q/\sqrt{v}$ - ratio. When taking into account the standard deviations, also the roughness values of these diagonals are approximately the same. This assessment suggests a strong correlation between the peak surface temperature T_p^* and the surface roughness.

For a semi-infinite body of isotropic material scanned (rescanned/remelted) with a moving gaussian laser beam, also an analytical model of laser surface hardening can be developed. Figure 12-a gives a model-based overview of laser surface hardening. In this figure the dimensionless

depth l^* represents the dimensionless height of the heat affected zone (HAZ) and is defined as $l^* = l/r_B$, where l is the depth of the HAZ. This depth can be defined as depth at which the underlying material has reached a predefined value. The value of the dimensionless depth increases when higher laser powers and lower scan speeds are used. This corresponds to the observation that when using a high remelting power and low scan speed, the porous support structure almost disappears by the increase of the heat affected zone (HAZ). Notice that also for stainless steel an increase in heat affected zone is observed when remelting with low scan speeds and high laser powers.

Figure 12-b is a laser hardening diagram for the steel 49MnVS3 treated with a beam of width 7mm and length 5mm. By taking into account empirical and theoretical equations for phase transformations in steels, hardness contours are obtained. This hardness contours reveal that a constant surface hardness can be obtained when using a low scan power together with a low scan speed or using a high scan power together with a higher scan speed. The surface hardness decreases when using a high laser power together with a low scan speed. When using a low scan power together with a high traverse rate no surface transformation and therefore no change in hardness occurs. All this observations correspond to the variations of surface hardness in Ti-6Al-4V, as seen in Figure 6. E.g. as seen in Figure 4, there is almost no improvent in surface roughness for the part rescanned with a low power of 64 W and a high scan speed of 1280 mm/s as compared to the reference parts. Therefore there is also no significant difference between the surface hardness of this part and the surface hardness of a reference part (see Figure 6).

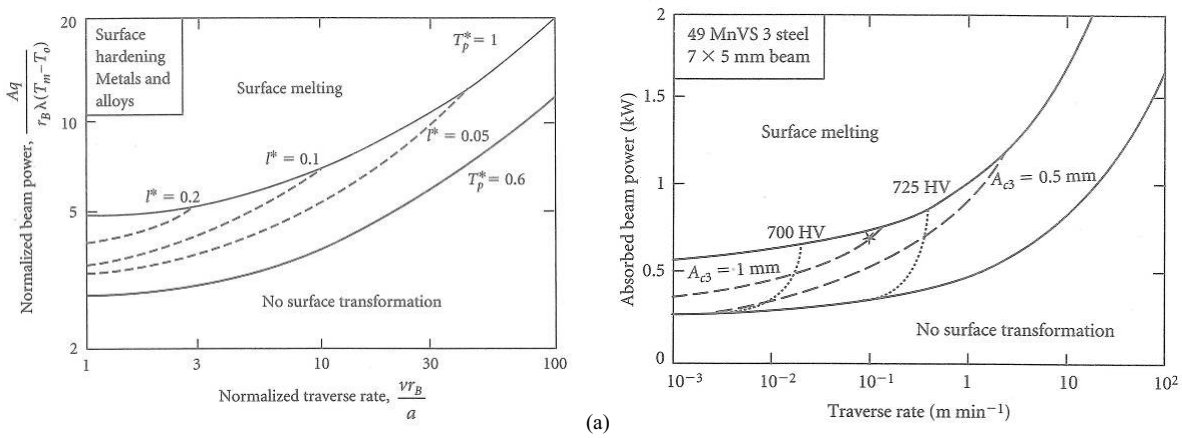

Figure 12. Model-based overview of laser surface hardening (a). Laser hardening diagram for the steel 49MnVS3 treated with a beam of width 7 mm and length 5 mm (b)[28].

CONCLUSIONS

This paper described the influence of Laser Surface Remelting on surface roughness, microhardness, wear behaviour and microstructure for titanium alloy (Ti-6Al-4V). Some results obtained for stainless steel (ASTM 316L) are also reported.

For titanium alloy, Laser Surface Remelting with optimized parameters for laser power and scan speed leads to a significant roughness improvement, without inducing edges at the contours of the produced parts. Note that in previous research, for stainless steel, remelting with optimized parameters even yielded a roughness improvement of 90% [3].

For titanium alloy, the LSR process increases the microhardness. For parts remolten with a certain remelting scan velocity, the wear volume of a fretting scar might be proportional to the hardness of the surrounding top surface. Also the thickness of the heat affected zone (HAZ)

increases for an increasing laser power and a decreasing remelting velocity. Especially for titanium alloy, but also for stainless steel, an analytical model is presented that matches with many of the observed results.

ACKNOWLEDGEMENTS

The authors thank IWT for the support through the SBO-project DiRaMaP and K.U.Leuven for the support through the project GOA/2002-06. Evren Yasa also acknowledges TUBITAK (The Scientific and Technological Research Council of Turkey) for its financial support given under the name of "Ph.D. support program for students in foreign countries".

REFERENCES

1. Kruth, J.P. 1991 Material incress manufacturing by Rapid Prototyping Techniques, Keynote paper. Annals of the CIRP 40(2):603-614.
2. Braga, F.J.C., Marques, R.F.C., Filho, E.A., Guastaldi, A.C., 2007. Surface modification of Ti dental implants by Nd:YVO_4 laser irradiation, Applied Surface Science 253: 9203-9208.
3. Yasa, E., Kruth, J.-P., Deckers, J., Roughness improvement in selective laser melting, 2008, PMI Conference, Ghent, Belgium, Sept.
4. Yasa, E., Kruth, J.-P., 2008. Experimental study of the combined process of selective laser melting and selective laser erosion, Proc. of RAPID2008 Conference, Florida, USA, May 20-22.
5. Henari, F.Z., Blau, W. 1995. Excimer-Laser Surface Treatment of Metals for Improved Adhesion. Applied Optics 34: 581–584.
6. Nicolas, G., Autric, M., Marine, W., Shafeev, G.A. 1997. Laser induced surface modifications on ZrO ceramics. Applied Surface Science 109-110: 289–292.
7. Triantafyllidis, D., Li, L., Stott, F.H. 2005. The effects of laser-induced modification of surface roughness of Al2O3-based ceramics on fluid contact angle. Materials Science and Engineering A 390: 271-277.
8. Lamikiz, A., Sanchez, J.A., Lopez de Lacalle, L.N., del Pozo, D. and Etayo, J.M., 2006, Surface roughness improvement using laser-polishing techniques, Materials Science Forum 526: 217-222.
9. Kac, S., Kusinki, J. 2004. SEM structure and properties of ASP2060 steel after laser melting. Surface and Coatings Technology. 180-181: 611-615.
10. Xianqing, Y., Chengjun, Z., Xuefeng, S., Manping, H., Jianguo, M. 2007. Microstructure evolution of WC/steel composite by laser surface re-melting. Applied Surface Science 253: 4409-4414.
11. Pinto, M.A., Cheung, N., Ierardi M.C.F., Garcia, A. 2003. Microstructural and hardness investigation of an aluminum-copper alloy processed by laser surface melting. Materials Characterization 50: 249-253.
12. Zhang, Y., Chen, J., Lei, W., Xv, R. 2008, Effect of laser surface melting on friction and wear behaviour of AM50 magnesium alloy. Surface and Coatings Technology 202: 3175-3179.
13. Felgueroso, D., Vijande, R., Cuetos, J.M., Tucho, R., Hernandez, A. 2008. Parallel laser melted tracks: Effects on the wear behaviour of plasma-sprayed Ni-based coatings. Wear 264: 247-263.
14. Kac, S., Kusinki, J. 2004. SEM structure and properties of ASP2060 steel after laser melting. Surface and Coatings Technology. 180-181: 611-615.

15. Zhang, Y., Chen, J., Lei, W., Xv, R. 2008. Effect of laser surface melting on friction and wear behavior of AM50 magnesium alloy. Surface and Coatings Technololgy 202: 3175-3179
16. Tang, C.H., Cheng, F.T., Man, H.C. 2004. Improvement in cavitation erosion resistance of a copper based propeller alloy by laser surface melting. Surface and Coatings Technology 182: 300-307.
17. Xu, W.L., Yue, T.M., Man, H.C., Chan, C.P. 2006. Laser surface melting of aluminium alloy 6013 for improving pitting corrosion fatigue resistance. Surface & Coatings Technology 200: 5077-5086.
18. Hao, L., Lawrence, J. 2006. Effects of Nd:YAG laser treatment on the wettability characteristics of a zirconia based bioceramic. Optics and Lasers in Engineering 44: 803-814.
19. Lawrence, J., Li, L. 2001. A laser based technique for the coating of mild steel with a vitreous enamel. Surface and Coatings Technology 140: 238-243.
20. Triantafyllidis, D., Li, L., Stott, F.H. 2005. The effects of laser-induced modification of surface roughness of Al2O3-based ceramics on fluid contact angle. Materials Science and Engineering A 390: 271-277.
21. Fouvry, S., Kapsa, P., Zahouani, H., Vincent L., 1997. Wear analysis in fretting of hard coatings through a dissipated energy concept. Wear 203-204: 393-403.
22. Duisabeau, L., Combrade P., Forest, B., 2004. Environmental effect on fretting of metallic materials for orthopaedic implants. Wear 256: 805-816.
23. Majumdar, J.D., Pinkerton, A., Liu, Z., Manna, I., Li, L., 2005. Microstructure characterization and process optimization of laser assisted rapid fabrication of 316L stainless steel. Applied Surface Science 247: 320-327.
24. Zhang, Y., Xi, M., Gao, S., Shi, L., 2003. Characterization of laser direct deposited metallic parts. Journal of Materials Processing Technology 142: 582-585.
25. Boyer, R., Welsch, G. Colling, E.W. 1994. Materials properties handbook: titanium alloys. Publisher: Materials Park (Ohio): ASM International, ISBN 0-87170-481-1.
26. Vandenbrouocke B., 2008. Selective Laser Melting of Biocompatible Metals for Rapid Manufacturing of Medical Parts, PhD thesis, K.U.Leuven, Department of Mechanical Engineering, Division PMA, Heverlee.
27. Searles, T. et al. Rapid characterisation of titanium microstructural features for specific modelling of mechanical properties, Meas. Sci. Technol. 16:60-69.
28. Kelly, S. M., and Kampe, S. L. ,2004. Microstructural evolution in laser-deposited multilayer Ti-M-4V builds: Part I. Microstructural characterization, Metallurgical and Materials Transactions; A; Physical Metallurgy and Materials Science, 35A(6), 1861 - 1867.
29. Kelly, S. M., and Kampe, S. L., 2004. Microstructural evolution in laser-deposited multilayer.
30. Qian, L., Mei, J., Liang, J., and Wu, X. ,2005. Influence of position and laser power on thermal history and microstructure of direct laser fabricated Ti-6Al-4V samples. Materials Science & Technology, 21(5), 597-605.
31. John Ion, 2005. Laser processing of engineering materials, Publisher: Elsevier, ISBN-13: 978-0-7506-6079-2.